IEICE TRANS. COMMUN., VOL.E96–B, NO.6 JUNE 2013

PAPER Special Section on Heterogeneous Networks for Future Cellular Systems

Interference Rejection Characteristics by Adaptive Array at User Equipment Using Measured *K*-Factor in Heterogeneous Networks

Kentaro NISHIMORI[†a)], ***Senior Member***, **Keisuke KUSUMI**[†], ***Student Member***, **Misaki HORIO**[†], ***Nonmember***, **Koshiro KITAO**[††], ***and*** **Tetsuro IMAI**[††], ***Members***

SUMMARY In LTE-Advanced heterogeneous networks, a typical cell layout to enhance frequency utilization is to incorporate picocells and femtocells in a macrocell. However, the co-channel interference between the marcocell and picocell/femtocell is an important issue when the same frequency band is used between these systems. We have already clarified how the interference from the femto(macro) cell affects on the macro(femto) cell. In this paper, we evaluate the interference rejection characteristics by an adaptive array with user equipment (UE). The characteristics are evaluated based on the *K*-factor used in the Nakagami-Race Fading model and the spatial correlation that is obtained in an actual outdoor environment. It is shown that a two-element adaptive array at the macro UE (M-UE) can sufficiently reduce the interference from the femto base station (F-BS) to the M-UE even if the number of total signals exceeds the degrees of freedom of the array.

key words: *heterogeneous networks, adaptive array, user equipment, K-factor, zero forcing*

1. Introduction

Due to the immense popularity of mobile phones and wireless LAN systems, increasing the data rate within a limited spectrum is a very important goal in wireless systems. Macrocells, the service areas for which are one to several kilometers, were introduced in conventional cellular systems. On the other hand, femto and picocells are currently a focus of attention because small cells can enhance the frequency utilization and can be established using a low-power-consuming base station (BS) that requires a small installation space. In Long Term Evolution (LTE)-Advanced, heterogeneous networks are extensively discussed in addition to traditional well-planned macrocell deployment to improve further the frequency utilization [1]–[3]. In heterogeneous network deployment, low power nodes such as femto, pico, and relay nodes are placed throughout a macrocell layout, and they are placed generally in an unplanned manner. Hence, interference between the macrocell and pico(femto)cells occurs because the transmission power of the pico(femto)cells is different from that of the macrocell and the service coverage areas are different between these cells. The picocells and femtocells are used in outdoor and indoor environments, respectively, and the cell size of a picocell is basically the same as that of a femtocell, because the transmission power levels are the same [2].

In order to avoid interference in the downlink between the macrocell and picocells, Cell Range Expansion (CRE) and Inter-Cell Interference Coordination (ICIC) were proposed [4]. These schemes can avoid the interference between the macrocell and picocells while a number of sets of user equipment (UEs) are connected to a picocell [4]. Since a femto BS (F-BS) has a function referred to as a Closed Subscriber Group (CSG), which allows only pre-registered UEs (femto UEs (F-UEs)), the macro UEs (M-UEs) that do not belong to the F-BS might receive/impart interference from/to the F-BS. Hence, in this paper, we focus on the interference between the F-BS and M-UE.

Since the BS antennas are allocated installation space, there have been many BS interference rejection techniques proposed and developed [5], [6]. Hence, the interference from the M-BS to F-BS can be suppressed using conventional techniques that employ an adaptive array at the F-BS when the BS is equipped with a sufficient number of antennas. Recently, the UE has been equipped with multiple antennas due to the popularity of Multiple Input Multiple Output (MIMO) systems [7], [8]. Interference rejection between multiple macrocells using a two element adaptive array at the UE was evaluated [9]. Moreover, since the downlink transmission rate is higher than that for the uplink, interference cancellation in the downlink (F-BS to M-UE) is more important than that in the uplink (M-UE to F-BS). Hence, we deal with interference rejection using an adaptive array at the UE between the macrocell and femtocells.

We evaluated Signal to Interference plus power Noise Ratio (SINR) characteristics using propagation characteristics such as path loss, shadowing, and penetration loss on outdoor to indoor propagation in heterogeneous networks [10]. This paper shows that the SINR with one element reception at the M-UE is less than 10 dB when the propagation from the F-BS to M-UE is regarded as a Line of Sight (LOS) environment.

In this paper, we investigate the SINR characteristics when using an adaptive array at the UE based on computer simulation using measured propagation parameters in heterogeneous networks. By using the received power with a two element array at the M-UE, we newly obtain the spatial correlation and *K*-factor used for the Nakagami-Race Fading model because these parameters greatly affect the interference rejection performance of the adaptive array [11],

Manuscript received October 12, 2012.
Manuscript revised February 1, 2013.

[†]The authors are with the Faculty of Engineering, Niigata University, Niigata-shi, 950-2102 Japan.
[††]The authors are with NTT DOCOMO, INC., Yokosuka-shi, 239-8536 Japan.
a) E-mail: nishimori@m.ieice.org

DOI: 10.1587/transcom.E96.B.1256

[12].

The path loss, shadowing, and penetration loss on outdoor to indoor propagation are utilized in [10] because the measurements in [10] use two antennas at the receiver site. Moreover, these propagation parameters are essential for an *exact* evaluation of the SINR in heterogeneous networks [10]. The computer simulation herein using these measured propagation parameters shows that the two element adaptive array at the M-UE greatly improved the SINR compared to one element reception. Moreover, we verify that the adaptive array efficiently suppresses *multiple* sources of interference between the F-BS and M-UE even if the total number of signals (desired signal plus interference) exceeds the degrees of freedom of the array antenna.

The rest of the paper is organized as follows. Section 2 describes the target scenario and defines the problem to be addressed. Section 3 presents the characteristics based on the K-factor and spatial correlation obtained at the Faculty of Engineering building of Niigata University, Japan. Section 4 describes the SINR characteristics with and without the adaptive array at the UE using the measured propagation parameters obtained in Sect. 3. Section 5 concludes the paper.

2. Target Scenario and Problem Definition

Figure 1 shows a configuration for heterogeneous networks in LTE-Advanced [1]. In such heterogeneous networks, picocells, femtocells, and relays are deployed inside the service area of a macrocell in order to enhance the frequency utilization and guarantee the quality of service in high traffic areas. The picocell service area is several tens of meters. Femtocells have drawn much attention recently because their transmission power level is very low and thus they only require a low-power-consuming BS and small installation space inside a building. The cell size of a femtocell is the same as that of a picocell because the transmission power levels are the same [2]

An important issue facing heterogeneous networks is achieving co-existence between the macrocell and pico(femto)cells that use the same frequency band, because 100 MHz broadband transmission is required in LTE-Advanced [13] and the frequency band is limited. However, when co-existence is employed between the macrocell and pico(femto)cells, interference between the macrocell and pico(femto)cells occurs because the transmission power and the service coverage area of the pico(femto)cells are different from those of the macrocell. Although ICIC and CRE [4] can be used to suppress the interference between the macrocell and picocells, the interference between the macrocell and femtocells cannot be avoided because the femtocell has the CSG function, which accommodates only pre-registered UEs (F-UEs) and the M-UE cannot employ pre-registration. The signal from/to the M-UE becomes interference [2]. In this paper, we focus on the interference between the macrocell and femtocells.

Figure 2 shows the interference between the macrocell and femtocells. The figure shows four kinds of interference sources between the macrocell and femtocells. Frequency Division Duplex (FDD), in which different frequencies are used between the BS (F-BS and macro BS : M-BS) and UE (F-UE and M-UE), is basically adopted in LTE-Advanced [13]. Regarding interference sources 3 and 4 in Fig. 2, the F-UE can select an appropriate BS (F-BS or M-BS) and avoid interference by using a channel allocation scheme such as ICIC [4], because the M-BS does not have the CSG function [2]. Since the aim of this paper is to evaluate the capability of the adaptive array at the M-UE using measured propagation parameters, we only deal with interference source 1.

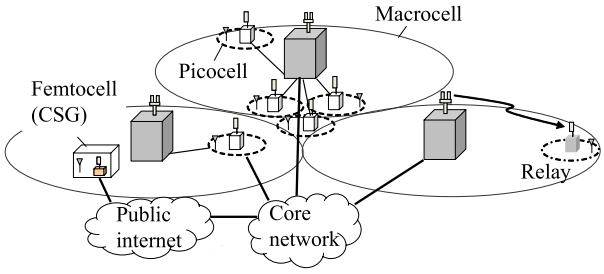

Fig. 1 Configuration of heterogeneous network.

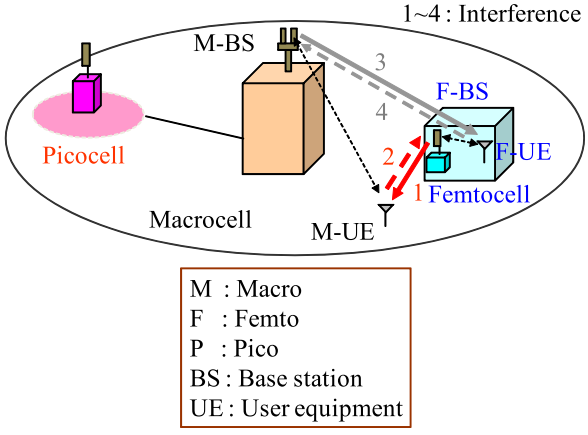

Fig. 2 Interference between macrocell and femtocells.

3. Measured K-Factor and Spatial Correlation in a Real Propagation Environment

3.1 Measurement Environment

In this section, the K-factor and spatial correlation are measured for the SINR evaluation using an adaptive array at the UE when considering the desired signal from the M-BS to the M-UE and the interference from the F-BS to the M-UE. Since there are M-UEs that do not belong to the CSG BS (F-BS), such M-UEs might impart/receive interference to/from the F-BS [1]. Moreover, the femtocell is generally used in indoor scenarios, and the propagation characteristics between the femtocell and macrocells are different from those inside a macrocell. We performed measurements to obtain the K-factor and spatial correlation between the fem-

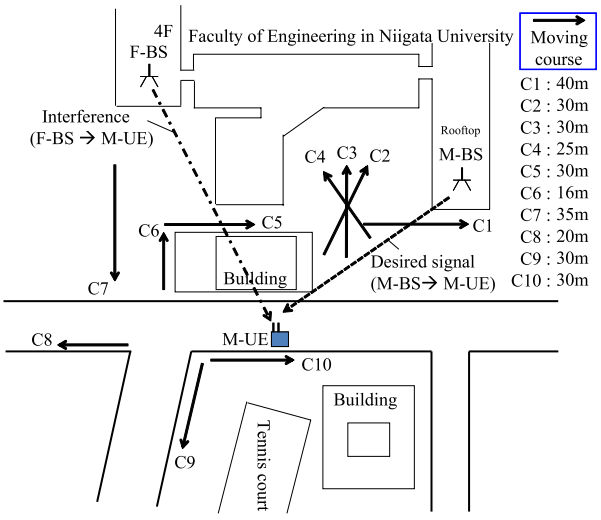

Fig. 3 Measurement environment.

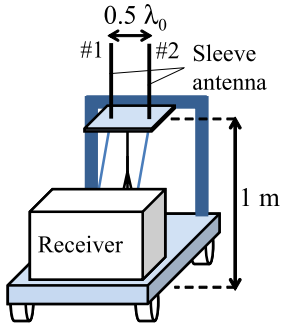

Fig. 4 Measurement configuration at M-UE.

tocell and macrocell and inside a macrocell, and reflected the results in the computer simulation described in Sect. 4.

Figure 3 shows the considered measurement environment. The measurements are taken in the Faculty of Engineering building of Niigata University in Japan. We assume the scenario where the interference from the F-BS arrives at the M-UE when the M-BS communicates with the M-UE. The radio frequency is 2.2 GHz and a continuous wave (10 W) is transmitted from the M-BS or F-BS to the M-UE. The number of transmitter antennas is one at the M-BS and F-BS. The M-UE is located in a parking area and moved around Courses 1 to 10 (C 1 to C 10) in Fig. 3. The M-BS and F-BS are located on the top of the 6 floor Faculty of Engineering building and the 4-th floor in Fig. 3, respectively. The antenna heights of the M-BS and F-BS are 22.5 and 16.5 m, respectively. The M-BS, F-BS, and M-UEs are equipped with sleeve antennas.

Figure 4 shows the measurement configuration at the M-UE. The height of the M-UE is 1 m. As shown in this figure, the element spacing of the two element linear array is set to $0.5\,\lambda_0$ (λ_0: wavelength). The receiver obtains the received power with the sampling rate of 5 ms.

The F-BS is located in the place in Fig. 5, because the influence of the shadowing is changed by the difference of

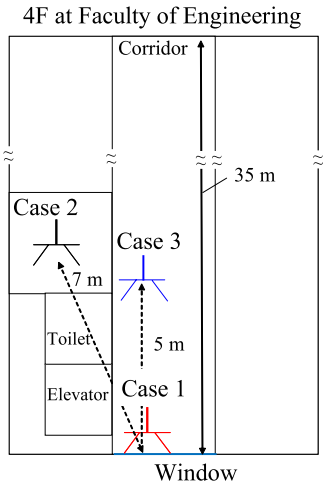

Fig. 5 Location of F-BS.

the place in Fig. 5 The location of the F-BS is indicated in Fig. 5. The influence of the shadowing changes with different locations. The figure shows that the antenna is located near a window in Case 1. The antenna is located inside the room in Case 2 and the distance between Case 1 and Case 2 is 7 m. The distance between Case 1 and Case 3 is 5 m.

We previously confirmed that the measured path loss for all the courses (C 1 to C 10) agrees fairly well with the C 2-LOS path loss model in WINNER II [14] when considering the path loss from the M-BS to M-UE [10]. On the other hand, based on the comparison between the measured path loss from the F-BS to the M-UE and the B 2-LOS path loss model in WINNER II [14], we confirmed that C 5 to C 8 and C 10 can be regarded as LOS and C 1 to C 4 and C 9 can be regarded as non-LOS (NLOS) [10].

3.2 Characteristics of K-Factor

We considered the Nakagami-Rice fading model as the propagation model. In this fading model, the propagation environment has one LOS path. The channel model is expressed as

$$\boldsymbol{H} = \sqrt{\frac{K}{K+1}}\boldsymbol{H}_{LOS} + \sqrt{\frac{1}{K+1}}\boldsymbol{H}_{NLOS}, \quad (1)$$

where $\boldsymbol{H}_{LOS}$ is a rank-one matrix corresponding to one LOS path, and $\boldsymbol{H}_{NLOS}$ represents a component of multipath scatters [11]. Then, K is the Rice factor, which has the strength of $\|\boldsymbol{H}_{LOS}\|^2$ relative to $\|\boldsymbol{H}_{NLOS}\|^2$ and characterizes the Nakagami-Rice distribution. Here, $\|\cdot\|$ denotes the Frobenius norm. When $K = 0$ ($-\infty$ [dB]), this model yields a Rayleigh distribution. $\boldsymbol{H}_{NLOS}$ denotes the channel matrix when considering independent and identically-distributed (i.i.d.) Rayleigh fading. The flow to obtain the K-factor and channel matrix is shown in Fig. 6. In the calculation in Fig. 6, the received power is calculated while changing the value of the K-factor. Step 4 in Fig. 6 is actually employed by the computer simulation in Sect. 4. The

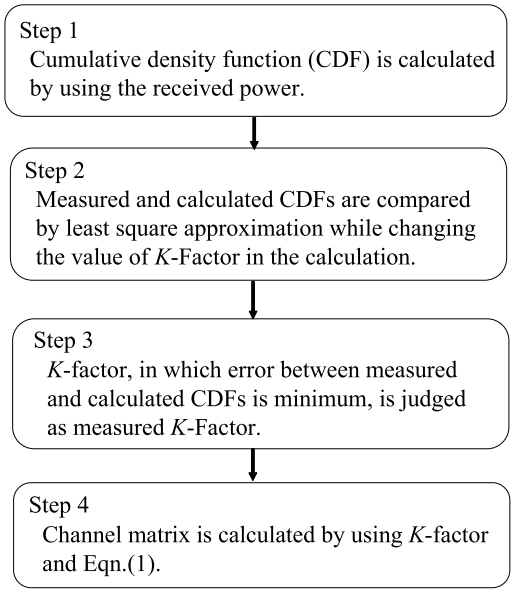

Fig. 6 Flow to obtain K-factor.

Table 1 Median values for K-factor.

	M-BS	F-BS [dB]		
	[dB]	Case 1	Case 2	Case 3
C1	1.51	0.59	0.59	−1.26
C2	−1.26	−2.18	−0.34	−1.26
C3	−1.26	−2.18	0.59	−1.26
C4	−1.26	−3.11	−2.18	−2.18
C5	−0.34	2.44	0.59	3.36
C6	−2.18	0.59	−2.18	1.51
C7	0.59	5.21	0.59	7.06
C8	−2.18	5.21	−3.11	5.21
C9	−1.26	−1.72	−0.34	−0.34
C10	−0.80	4.29	0.59	3.36

K-Factor is obtained using the received power corresponding to the interval of $10\,\lambda_0$ (λ_0: wavelength).

Table 1 shows the median values of the K-factor when considering all the courses for the M-BS/M-UE and F-BS/M-UE (Cases 1 to 3). As shown in Table 1, the K-factor is less than 6 dB except for C 7 of Case 3. Regarding C 5, C 7, and C 8 in Cases 1 and 3, K-factors higher than those in the other courses are observed because the perfect LOS environment is guaranteed at C 5, C 7, and C 8 as shown in Fig. 3. These results indicates that Rayleigh fading is appropriate as the propagation environment when considering both the desired signal in the macrocell and interference from the femtocell to macrocell.

Figure 7 shows the Cumulative Density Function (CDF) of the K-Factor when the results on all the courses are combined. The results on the M-BS/M-UE and F-BS/M-UE (Cases 1, 2, and 3) are compared in Fig. 7. The figure shows that the distributions are almost the same between the M-BS/M-UE and F-BS/M-UE (Cases 1, 2, and 3). The median values from the M-BS/M-UE and F-BS/M-UE (Cases 1, 2, and 3) are −0.33, 0.59, −0.33, and 0.58, respectively. Hence, the K-factor is very small regardless of the cell configuration even if a LOS environment is considered in heterogeneous networks.

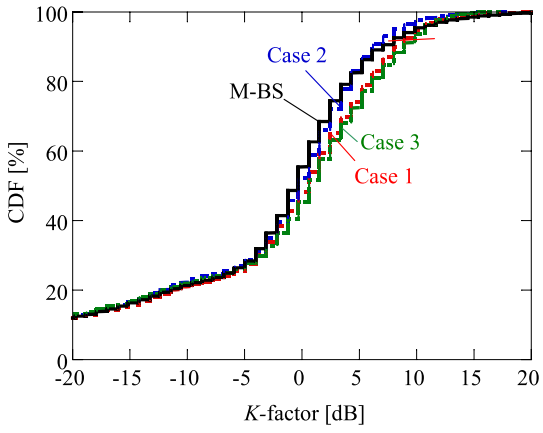

Fig. 7 Cumulative Density Function (CDF) of K-factor (M-BS, F-BS (Cases 1, 2, and 3).

3.3 Spatial Correlation Characteristics

When using (1) as the channel matrix, the assumption of the second term on the right side in (1) is very important because i.i.d. is assumed in (1) but a high spatial correlation might be observed in an outdoor scenario, especially at the BS site [15], [16]. Hence, we measured the spatial correlation at the M-UE. Since the received powers of antennas 1 and 2 are obtained in this measurement, the spatial correlation is expressed as

$$\rho = \frac{\left|\frac{1}{L}\sum_{i=1}^{L}\left(R_1(i)-\overline{R_1}\right)\left(R_2(i)-\overline{R_2}\right)\right|}{\sqrt{\frac{1}{L}\sum_{i=1}^{L}\left(R_1(i)-\overline{R_1}\right)^2}\sqrt{\frac{1}{L}\sum_{i=1}^{L}\left(R_2(i)-\overline{R_2}\right)^2}}, \quad (2)$$

$$\overline{R_k} = \frac{1}{L}\sum_{i=1}^{L} R_k(i) \ \ (k=1,2), \quad (3)$$

where $R_1(i)$ and $R_2(i)$ denote the instantaneous received powers at antennas 1 and 2, respectively. $\overline{R_1}$ and $\overline{R_2}$ are the averaged received powers at antennas 1 and 2, respectively, using L samples. In this measurement, $\overline{R_1}$ and $\overline{R_2}$ are actually obtained by the number of samples corresponding to the interval of $10\,\lambda_0$. L is approximately 2,500 because the sampling rate of the receiver is 5 kHz and the moving speed of the M-UE is $20\,\lambda_0$/s.

Figure 8 shows the spatial correlations using (2) and (3) when considering the received powers of the M-BS/M-UE and F-BS/M-UE (Cases 1 to 3). Generally speaking, the complex channel vector should be used to evaluate the adaptive array with spatial correlation [12]. We compared the spatial correlation using the complex channel vector to that using (2) based on measured data. When 2×1 complex channel vectors for the desired signal and interference are $\boldsymbol{h}_S$ and $\boldsymbol{h}_I$, respectively, spatial correlation ρ_c is calculated

as

$$\rho_c = \frac{\boldsymbol{h}_S^H \boldsymbol{h}_I}{\sqrt{\|\boldsymbol{h}_S\|^2}\sqrt{\|\boldsymbol{h}_I\|^2}}. \quad (4)$$

For reference, $|\rho_c|^2$ is plotted in Fig. 8 when i.i.d. is assumed for $\boldsymbol{h}_S$ and $\boldsymbol{h}_I$. The reason why $|\rho_c|^2$ is used instead of $|\rho_c|$ in (4) is that (2) denotes the correlation using power and not amplitude. Figure 8 shows that the spatial correlations based on the measurement results are lower than those based on the calculated results when considering i.i.d. in (4).

The 90% CDF values for the spatial correlation are plotted in Fig. 9 considering each measurement course, because the bad condition should be evaluated when considering the system evaluation [11]. From the results in Fig. 8, since the spatial correlation based on Case 1 is almost the same as that for Case 3, the results in Case 1 are plotted in Fig. 9. As shown in Fig. 9, the spatial correlations based on the measured results are smaller than the spatial correlation, $|\rho_c|^2$, regardless of the measurement course. Although the definition using (2) and (3) is different from that using (4), it is shown that the measured spatial correlation indicates that the propagation environment with the array antenna at the M-UE can be regarded as i.i.d. The assumption of the second term on the right side in (1) can be properly used for the evaluation of the M-UE in heterogeneous networks.

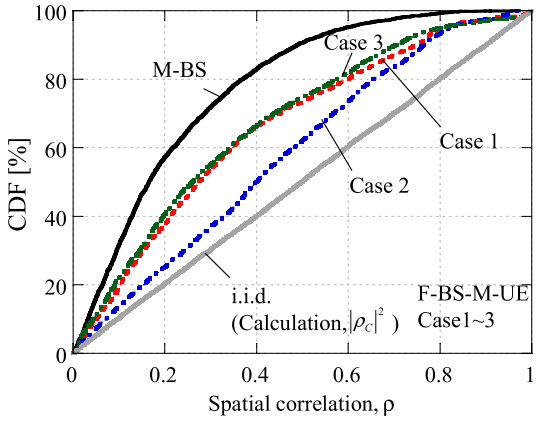

Fig. 8 CDF of spatial correlation (M-BS, F-BS (Cases 1 to 3).

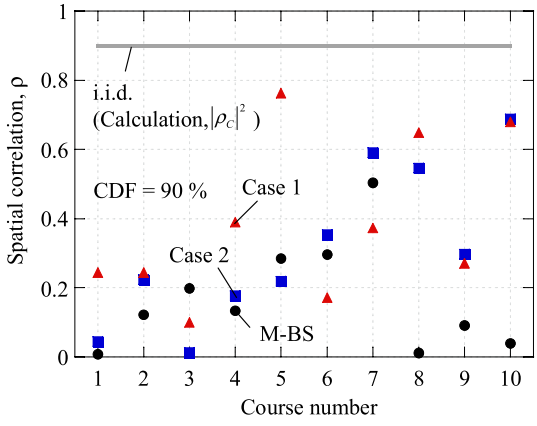

Fig. 9 Spatial correlation versus measured course number (M-BS, F-BS (Cases 1 and 2).

4. Effectiveness of UE Adaptive Array Using Measured *K*-Factor

From the measurement results regarding the *K*-factor and spatial correlation, it is shown that (1) can be properly used to evaluate the M-UE in heterogeneous networks. In this section, the SINR is evaluated when considering the adaptive array at the M-UE using the measured *K*-factor and propagation parameters in [10].

The SINR is evaluated using the measured propagation parameters at only one location. Moreover, since the simulation parameters are limited in this study, the measurement at other locations and simulations using various parameters will be required for a more exact evaluation. Hence, this simulation in this study is regarded as a case study.

4.1 Simulation Environment

Tables 2 and 3 show the propagation and simulation parameters, respectively, for the evaluation of interference rejection using an adaptive array at the M-UE. The parameters in Table 2 are cited from [10] because the measurement location herein is the same as that in [10]. Since we confirmed that the measured path loss agrees well with that from the WINNER II model [10], the path loss from the WINNER II model is adopted in this evaluation. The parameters in Table 3 basically follow those in [2], because the parameters are used in the standardization evaluation for LTE-Advanced. The noise power is actually −104 dBm, because the bandwidth is assumed to be 10 MHz in this paper.

Figure 10 shows an example of the positional relationship between the macrocell and femtocells. The numbers of macrocells (N_M) and femtocells (N_F) are one and three, respectively. Although multiple macrocells should be taken into account in a precise evaluation, a single cell for the

Table 2 Propagation parameters.

Parameter	Value
Path loss (M-BS, M-UE, LOS)	Model C2 [14]
Path loss (F-BS, M-UE, LOS)	Model B1 [14]
Path loss (F-BS, M-UE, NLOS)	Model B1 [14] + 20 dB
Path loss indoors	10.9 dB [10]
Wall penetration	5.6 dB [10]
Std. of small fading	Measured results [10]
K-factor	Measured results

Table 3 Simulation parameters.

Parameter	Macrocell	Femtocell
Cell radius	289 [m]	40 [m]
BS Tx power	46 [dBm]	30 [dBm]
BS ant. gain	14 [dBi]	5 [dBi]
UE ant. gain	0 [dBi]	0 [dBi]
Noise power	−174 [dBm/Hz]	−174 [dBm/Hz]
Height (BS)	22.5 [m]	16.5 [m]
Height (UE)	1.0 [m]	–

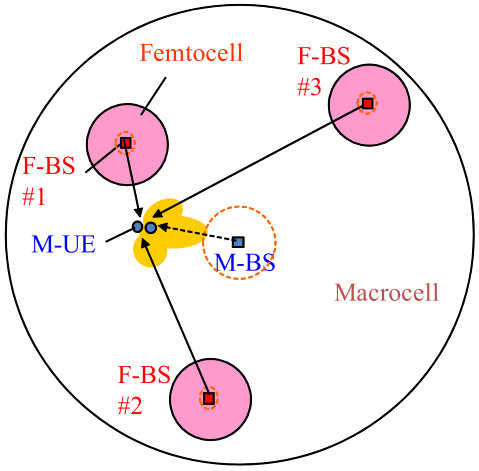

Fig. 10 Example layout of macrocell and femtocells (Number of femtocells, $N_F = 3$).

macrocell is assumed in this paper to consider multiple interference sources that are purely only from F-BSs as shown in Fig. 10. The number of F-BSs is set to one to four in the simulation. The SINR is calculated using an adaptive array at the M-UE, when changing the location of the M-UE and F-BSs. The number of trials is set to 10,000 and the CDF of the SINR is obtained. The SINR is expressed as

$$\text{SINR} = \frac{P_S}{P_I + P_N}, \tag{5}$$

where P_S, P_I, and P_N denote the desired signal, interference, and noise power, respectively.

The distribution of the K-factors obtained in Fig. 7 are reflected in the simulation. The channel matrix is calculated using (1). When the two element array at the M-UE and one desired signal and interference are assumed in (1), $\boldsymbol{H}_{LOS}$ is expressed as

$$\boldsymbol{H}_{LOS} = \begin{pmatrix} G_s & G_i \\ G_s e^{-j2\pi/\lambda_0 d \sin\theta_S} & G_i e^{-j2\pi/\lambda_0 d \sin\theta_I} \end{pmatrix}, \tag{6}$$

where θ_S and θ_I denote the direction of arrival for the desired signal and the interference, respectively, and these values are given according to the location of the F-BS and M-UE in each trial. Term d is the element spacing and is $0.5\,\lambda_0$ in the simulation. Terms G_s and G_i denote the gain due to the path loss, respectively.

As the principle for the adaptive array, zero forcing (ZF), which is known as a simple decoding method for adaptive arrays and MIMO transmission, is adopted. Using the Minimum Mean Square Error (MMSE) criterion is proposed to reduce the interference according to the interference power. The received signal and reference signal for the desired signal are required in the MMSE algorithm. It is shown that the SINR by MMSE outperforms compared to that by ZF [17]. However, there is an issue when using the MMSE when considering the control signal in LTE-Advanced because the Space Frequency Block Code (SFBC) is used in the control signal, and the MMSE must handle two signals for each symbol. From the viewpoint of the degrees of freedom at the array antenna, employing MMSE for interference cancellation is not suitable.

Although it is generally difficult to obtain a channel response regarding the interference, the control signal can be utilized not only for the desired signal but also for the interference because we assume a "single" radio interface based on LTE-Advanced between the macrocell and femtocell [4]. Moreover, the interference cancellation using the control signals between the marcocell and picocell in LTE-Advanced was proposed [18]. It is shown in [18] that the control signals for the macrocell and picocell at the M-UE can be obtained, although the interference between the macrocell and picocells occurs during the data period. In addition, multiple control signals are used to cancel multiple interfering signals in [9].

However, since a two element adaptive array is considered, the adaptive array cannot cancel the interference when there are more than two signals. To address this problem, we propose the following scheme.

Step 1 The 2×1 channel vector, $\boldsymbol{h}_{I_1}$, which is the interference from the F-BS to M-UE with the highest power among all the interfering sources, is estimated.
Step 2 The weight of ZF is calculated using $\boldsymbol{h}_{I_1}$ obtained in Step 1 and $\boldsymbol{h}_S$ which is the 2×1 channel vector between the M-BS and M-UE.
Step 3 The SINR is calculated using the weight in Step 2.

When using an adaptive array and the above steps, P_S, P_I, and P_N are given as

$$P_S = E\left[|\boldsymbol{w}_S^T \boldsymbol{h}_S\, s_d(t)|^2\right], \tag{7}$$

$$P_N = E\left[|\boldsymbol{w}_S^T \boldsymbol{n}(t)|^2\right], \textit{and} \tag{8}$$

$$P_I = E\left[|\boldsymbol{w}_S^T \boldsymbol{h}_{I_1} i_1(t)|^2 + \sum_{k=2}^{N_F} |\boldsymbol{w}_S^T \boldsymbol{h}_{I_k} i_k(t)|^2\right], \tag{9}$$

where $\boldsymbol{w}_S$ is the weight of ZF for the interference rejection. Terms $s_d(t)$ and $i_k(t)$ ($k = 1 \sim N_F$) are the desired signal and k-th interference, respectively, at time index t. Term $\boldsymbol{n}(t)$ is the thermal noise vector at the receiver. For the interference power, P_I, note that the first term on the right side is zero but the second term exists as residual interference. Term $E[\cdot]$ is the expectation value and five samples are used to obtain P_S, P_I, and P_N instead of using $E[\cdot]$, four samples at least are required for the calculation of weight on the two element adaptive array [19]. Channel vectors ($\boldsymbol{h}_S$ and $\boldsymbol{h}_{I_1}$) are obtained using the least square method with five samples.

4.2 SINR Characteristics of UE Adaptive Array

Figure 11 shows the CDF of the SINR when a two element adaptive array is applied to the M-UE. The power differences between Cases 1 and 2 and Cases 1 and 3 in Fig. 5 are obtained based on the measurement results and the median values are 5.6 and 10.9 dB, respectively. The number of F-BSs (N_F) is set to 2 in Fig. 11. Since the total number of sig-

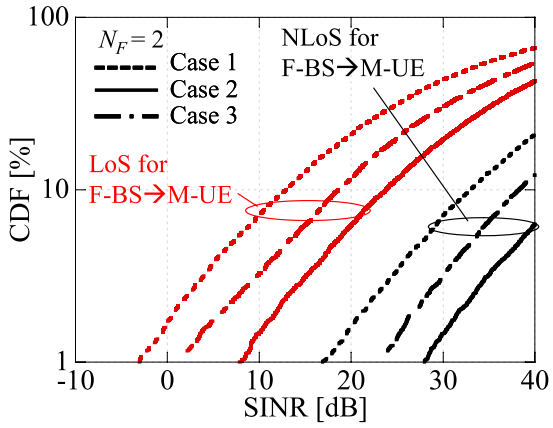

Fig. 11 CDF of SINR (N_F = 2).

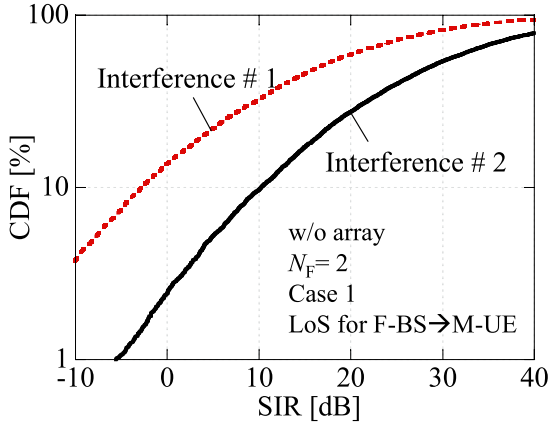

Fig. 12 CDF of SIR (N_F = 2, Case 1, LOS for F-BS to M-UE).

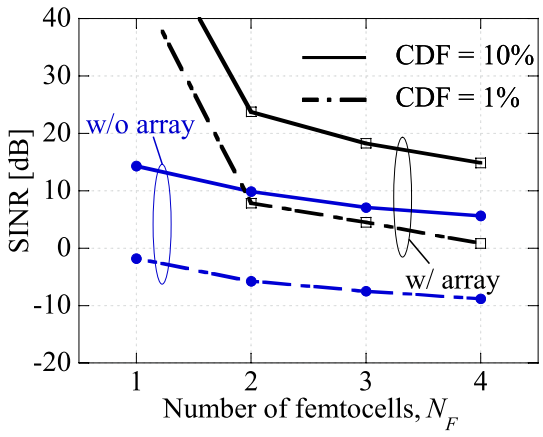

Fig. 13 SINR versus sources of interference (LOS, Case 2).

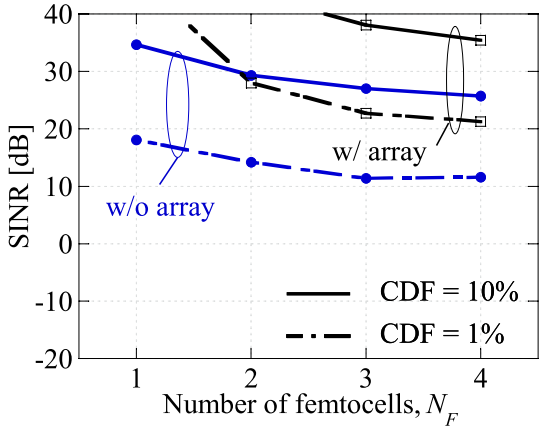

Fig. 14 SINR versus sources of interference (NLOS, Case 2).

nals exceeds the number of antennas at the M-UE, the adaptive array cannot completely cancel the interference. However, as shown in Fig. 11, the SINR is greater than 10 dB even when an outdoor LOS environment between the F-BS and the M-UE in Case 1 is considered.

In order to understand the reason why the high SINR is obtained, the Signal to Interference power Ratio (SIR) without the array antenna is plotted in Fig. 12 when considering Case 1 and a LOS scenario for the F-BS to M-UE under outdoor propagation conditions. Interference sources #1 and #2 in Fig. 12 denote the interference sources with higher and lower power, respectively. Figure 12 shows that since there is a power difference between interference sources #1 and #2, the proposed scheme can be used to reject the dominant interference. In the case of Fig. 12, interference source #1 can be completely cancelled by ZF. On the other hand, the SIR is approximately 10 dB for interference source #2 at 10% of the CDF and the SINR with the adaptive array is almost 13 dB due to the array gain as shown in Fig. 11, although the proposed scheme does not employ nulling for interference source #2. One problem with the ZF algorithm is that the desired signal decreases in power due to the interference cancellation when the spatial correlation between the desired and interfering signals is very high. However, when using the proposed scheme the desired signal does not decrease in power due to interference cancellation because the K-factor is very small and the spatial correlation between the desired and interfering signals is very low. Hence, it is shown that the two element adaptive array at the M-UE obtains a sufficient SINR by cancelling only one source of interference with the highest power level among multiple interference sources when considering the propagation environment in heterogeneous networks.

Figures 13 and 14 show the SINR characteristics versus the number of interference sources in outdoor LOS and NLOS environments between the F-BS and M-UE, respectively. Case 2 is assumed as the setting for the F-BS. The 1% and 10% values of the CDFs are plotted in these figures. The figures show that the adaptive array at the M-UE can achieve a 9-dB improvement in the SINR compared to one element reception, even if the total number of signals exceeds the degrees of freedom at the array antenna. As shown in Fig. 13, the SINR is greater than 14 dB even in the outdoor LOS environment with four sources of interference, which is the most severe environment in the simulation.

5. Conclusion

This paper investigated the SINR characteristics when using an adaptive array at the M-UE based on the measured K-factor in heterogeneous networks. From the measurement results at the M-UE when considering an environment in a heterogeneous network, we observed that the K-factor is less than 6 dB in almost all measurement courses regardless of the M-BS/M-UE and F-BS/M-UE. Moreover, we showed that the spatial correlation between two antennas is very low at the M-UE and the propagation between two antennas at the M-UE is regarded as i.i.d. Based on computer simulation using measured propagation parameters, we showed that a two element adaptive array achieves a 9-dB improvement in the SINR compared to one element reception when there are 4 sources of interference. Moreover, we clarified that the adaptive array at the M-UE efficiently reduces the interference between the F-BS and M-UE even if the total number of signals exceeds the degrees of freedom at the array by applying ZF to nullify the source of interference with the highest power level because each power level among the interfering sources is different.

Although, in this paper, a single antenna is assumed for the transmitter at the BS for the desired signal and interference, MIMO transmission and multiple MIMO interference should be considered in future work because MIMO transmission is now incorporated into LTE and is an important fundamental technology in LTE-Advanced.

In this study, the F-BS is assumed to be randomly located inside the service area in the M-BS by using the model described in [2]. On the other hand, many F-BSs will be located inside one building when considering an area with heavier traffic. Since multiple interfering signals with almost the same power simultaneously arrive at the M-UE, the performance of a two element adaptive array at the M-UE should be evaluated in such a scenario.

As for other future work, evaluation of broadband transmission with multiple macrocells is essential. The frequency correlation characteristics should be evaluated because these enable evaluation using exact propagation parameters in broadband Orthogonal Frequency Division Multiplexing (OFDM) systems [20]. Moreover, frequency correlation characteristics will help the evaluation using the K-factor because the results using the K-factor can be regarded as those at each subcarrier in the OFDM systems, and the frequency correlation characteristics and K-factor can be combined as parameters in evaluating broadband transmission.

References

[1] 3GPP, TR 36.814 (V9.0.0), "Further advancements for E-UTRA physical layer aspects," March 2010.
[2] M. Tanno, A. Morimoto, T. Abe, Y. Kishiyama, and T. Nakamura, "Heterogeneous network in LTE-advanced," IEICE Technical Report, RCS2009–317, March 2010.
[3] A. Khandekar, N. Bhushan, J. Tingfang, and V. Vanghi, "LTE Advanced: Heterogeneous networks," European Wireless 2010, pp.978–982, April 2010.
[4] M. Shirakabe, A. Morimoto, and N. Miki, "Performance evaluation in heterogeneous networks employing time-domain inter-cell interference coordination and cell range expansion for LTE-advanced downlink," IEICE Trans. Commun., vol.E95-B, no.4, pp.1218–1229, April 2012.
[5] Y. Ogawa and T. Ohgane, "Advances in adaptive antenna technologies in Japan," IEICE Trans. Commun., vol.E84-B, no.7, pp.1704–1712, July 2001.
[6] N. Kikuma and M. Fujimoto, "Adaptive antennas," IEICE Trans. Commun., vol.E86-B, no.3, pp.968–979, March 2003.
[7] G.J. Foschini and M.J. Gans, "On limits of wireless communications in a fading environment when using multiple antennas," Wireless Pers. Commun., vol.6, pp.311–335, 1998.
[8] D. Gesbert, M. Shafi, D. Shui, P.J. Smith, and S.A. Naguib, "From theory to practice: An overview of MIMO space-time coded wireless systems," IEEE J. Sel. Areas Commun., vol.21, no.3, pp.281–302, March 2003.
[9] Y. Ohwatari, N. Miki, T. Asai, T. Abe, and H. Taoka, "Performance of advanced receiver employing interference rejection combining to suppress inter-cell interference in LTE-advanced downlink," Proc. VTC Fall, Sept. 2011.
[10] K. Nishimori, S. Komatubara, K. Kitao, and T. Imai, "Measurements of propagation characteristics on outdoor, indoor and outdoor-indoor environment for evaluation on interference in heterogeneous networks," IEICE Trans. Commun. (Japanese Edition), vol.J95-B, no.9, pp.1159–1170, Sept. 2012.
[11] A. Paulaj, R. Nabar, and D. Gore, Introduction to space-time wireless communications, Cambridge University Press, 2003.
[12] H. Lin, "Spatial correlations in adaptive array," IEEE Trans. Antennas Propag., vol.30, no.2, pp.212–223, March 1982.
[13] 3GPP, TS 36.201 (V10.0.0), "Evolved universal terrestrial radio access (E-UTRA); LTE physical layer; General description (Release 10)," Dec. 2010.
[14] WINNER II channel models, http://www.ist-winner.org/deliverables.html
[15] K. Nishimori, Y. Makise, M. Ida, R. Kudo, and K. Tsunekawa, "Channel capacity measurement of 8×2 MIMO transmission by antenna configurations in an actual cellular environment," IEEE Trans. Antennas Propag., vol.54, no.11, pp.3285–3291, Nov. 2006.
[16] K. Nishimori, N. Honma, T. Murakami, and T. Hiraguri, "Effectiveness of relay MIMO transmission by measured outdoor channel state information," IEEE Trans. Antennas Propag., vol.60, no.2, pp.615–623, 2012.
[17] K. Nishimori, K. Kusumi, K. Kitao, and T. Imai, "Interference reduction characteristics by UE array antenna with ZF/MMSE criteria using real propagation data in heterogeneous networks," Proc. Commun. Conf. IEICE 2012, BS-1-8, Sept. 2012.
[18] M. Miyashita, M. Manabu, and H. Yoshino, "A study on inter-cell interference canceller for downlink L1/L2 control channel in LTE/LTE-advanced," Proc. Commun. Conf. IEICE 2012, B-5-68, Sept. 2012.
[19] R.A. Monzingo, R.L. Haupt, and T.W. Miller, Introduction to Adaptive array, 2nd ed., SciTech Publishing, 2011.
[20] K. Nishimori, N. Tachikawa, Y. Takatori, R. Kudo, and K. Tsunekawa, "Frequency correlation characteristics due to antenna configurations in broadband MIMO transmission," IEICE Trans. Commun., vol.E88-B, no.6, pp.2348–2445, June 2005.

Kentaro Nishimori received the B.E., M.E. and Ph.D. degrees in electrical and computer engineering form Nagoya Institute of Technology, Nagoya, Japan in 1994, 1996 and 2003, respectively. In 1996, he joined the NTT Wireless Systems Laboratories, Nippon Telegraph and Telephone Corporation (NTT), in Japan. He was senior research engineer on NTT Network Innovation Laboratories. He is now associate professor in Niigata University. He was a visiting researcher at the Center for Teleinfrastructure (CTIF), Aalborg University, Aalborg, Denmark from Feb. 2006 to Jan. 2007. He was an Associate Editor for the Transactions on Communications for the IEICE Communications Society from May 2007 to May 2010 and Assistant Secretary of Technical Committee on Antennas and Propagation of IEICE from June 2008 to May 2010. He received the Young Engineers Award from the IEICE of Japan in 2001, Young Engineer Award from IEEE AP-S Japan Chapter in 2001, Best Paper Award of Software Radio Society in 2007 and Distinguished Service Award from the IEICE Communications Society in 2005, 2008 and 2010. His main interests are spatial signal processing including MIMO systems and interference management techniques in heterogeneous networks. He is a member of IEEE. He received IEICE Best Paper Award in 2010.

Keisuke Kusumi received the B.E. degree from faculty of engineering in Niigata University in 2012. He is currently studying M.S. degree at graduate school of science and technology in Niigata University. His research interests are evaluation on interference and interference cancellation techniques in heterogeneous networks.

Misaki Horio is currently studying B.E. degree at faculty of engineering in Niigata University Her research interest is evaluation on interference in heterogeneous networks.

Koshiro Kitao was born in Tottori, Japan, in 1971. He received B.S., M.S. and Ph.D. degrees from Tottori University, Tottori, Japan in 1994, 1996 and 2009 respectively. He joined the Wireless Systems Laboratories, Nippon Telegraph and Telephone Corporation (NTT), Kanagawa, Japan, in 1996. Since then, he has been engaged in the research and development of radio propagation for mobile communications. He is now Assistant Manager of the Radio Access Network Development Department, NTT DOCOMO, INC., Kanagawa, Japan. Dr. Kitao is a member of the IEEE.

Tetsuro Imai was born in Tochigi, Japan, in 1967. He received his B.S. and Ph.D. degrees from Tohoku University, Japan, in 1991 and 2002, respectively. He joined the Wireless System Laboratories of Nippon Telegraph and Telephone Corporation (NTT), Kanagawa, Japan, in 1991. Since then, he has been engaged in the research and development of radio propagation, antenna systems and system design for mobile communications. He is now Manager of the Radio Access Network Development Department, NTT DOCOMO, INC., Kanagawa, Japan. He received the IEICE Young Researcher's Award in 1998 and the IEICE Best Paper Award in 2006. Dr. Imai is a Member of the the IEEE.